Ferroelectrics Letters Section

ISSN: 0731-5171 (Print) 1563-5228 (Online) Journal homepage: https://www.tandfonline.com/loi/gfel20

To study the effect of low temperature crystal growth on the structural and ferroelectric properties of lead-free BCT-BZT ceramic

Shweta Thakur, Mamta Shandilya, Manuel Pedro Fernanades Graça & Manuel Almeida Valente

To cite this article: Shweta Thakur, Mamta Shandilya, Manuel Pedro Fernanades Graça & Manuel Almeida Valente (2020) To study the effect of low temperature crystal growth on the structural and ferroelectric properties of lead-free BCT-BZT ceramic, Ferroelectrics Letters Section, 47:4-6, 76-89, DOI: 10.1080/07315171.2020.1810985

To link to this article: https://doi.org/10.1080/07315171.2020.1810985

FERROELECTRICS LETTERS SECTION
2020, VOL. 47, NOS. 4–6, 76–89
https://doi.org/10.1080/07315171.2020.1810985

Taylor & Francis
Taylor & Francis Group

To study the effect of low temperature crystal growth on the structural and ferroelectric properties of lead-free BCT-BZT ceramic

Shweta Thakur[a], Mamta Shandilya[b], Manuel Pedro Fernanades Graça[c], and Manuel Almeida Valente[c]

[a]Department of Physics, Akal College of Basic Sciences, Eternal University, HP, India; [b]School of Physics, Shoolini University, Solan, HP, India; [c]I3N-Aveiro, Department of Physics, University of Aveiro, Aveiro, Portugal

ABSTRACT

Barium Zirconate Titanate-Barium Calcium Titanate (BCT-BZT) is one of the lead-free systems, which exhibits remarkable ferroelectric properties akin to lead-based perovskite materials. In this study, we have synthesized $x(Ba_{0.85}Ca_{0.15})TiO_3$-$(1-x)Ba(Zr_{0.15}Ti_{0.85})O_3$ (where $x = 0.4$, 0.5, 0.6) monophonic powders by hydrothermal method at 150 °C. X-ray diffraction reveals the pure tetragonal phase. Scanning electron microscopy (SEM) studies make known that the crystal growth is uniform due to low temperature, and that the ceramics are highly dense and polycrystalline. The single semicircle indicates bulk behavior. The bulk resistance decreases with the increase in temperature showing a typical semiconducting property, negative temperature coefficient of resistance (NTCR) behavior.

ARTICLE HISTORY
Received 18 November 2019
Accepted 14 July 2020

KEYWORDS
BCT-BZT; dielectric properties; ferroelectricity; impedance spectroscopy

1. Introduction

The toxic chemical exposure from ceramics to the environment is a very significant concern. The demand for materials technology is increasing day by day; therefore, material and synthesis of materials should be environmentally benign [1,2]. Ferroelectrics are one of the emerging materials for applications in the field of ultrasonic devices, multilayer ceramic capacitors (MLCCs), electro-optic devices, energy harvesters, and piezoelectricity. Lead zirconate titanate materials have been commercially used material due to their excellent ferroelectric and piezoelectric properties, but these materials are toxic and volatile in nature and hence pose a threat to our environment. In order to eradicate lead-based technology, researchers have shifted their focus toward lead-free materials. Among various lead-free ferroelectric material, barium titanate ($BaTiO_3$) has been given a significant amount of attention because of its intriguing properties and high dielectric constant [3]. Doping at A-site and B-site improves its electromechanical and physical properties. Therefore, they have the potential to become an alternative to the PZT-based system, which has been used for sensors, transducers,

CONTACT Mamta Shandilya mamta2882@gmail.com
Communicated by Dr. George W. Taylor

motors, etc. [4,5]. Moving forward in this direction, Liu and Ren et al. [6] proposed the very first lead-free $x\mathrm{Ba}(\mathrm{Zr}_{0.2}\mathrm{Ti}_{0.8})\mathrm{O}_3$-$(1-x)(\mathrm{Ba}_{0.7}\mathrm{Ca}_{0.3})\mathrm{TiO}_3$ ($x = 0.5$) ceramics (hereafter abbreviated as BZT-BCT) by using the conventional solid-state route in which they highlighted the presence of high piezoelectric properties similar to that of lead-based materials. The Ca-modified material shows improved temperature stability in terms of the temperature coefficient of dielectric permittivity and a wider temperature range of stability [7,8]. On the other hand, doping of Zr^{4+} leads to an increase in transition temperature from orthorhombic to the tetragonal phase transition, while it decreases from tetragonal to cubic; it results, high dielectric gain [9,10].

BZT-BCT is reported to have a phase diagram similar to the Pb-based lead zirconate titanate (PZT), lead magnesium niobate lead titanate (PMN-PT) and lead nickel niobite-lead zirconate titanate (PNN-PZT), that is, morphotropic phase boundary (MPB) consists a triple point of ferroelectric rhombohedral (R), tetragonal (T) phase, and paraelectric cubic (C) phase [11]. Hence, BZT-BCT is presently one of the most substantial candidates for many piezoelectric applications due to its lead-free nature with an MPB similar to lead-based systems and with superior piezoelectric properties reported in the literature[12]. However, one issue suppressing their utilization for a commercial purpose is the preparation or synthesis process of very fine and homogeneous powders of high-purity and to assess a simpler and eco-friendly synthesis process in the laboratory [13]. Therefore, in this work, the hydrothermal method at low temperature (~100 °C–200 °C) was employed to obtain materials under thermodynamic conditions (Fig. 1). The hydrothermal method has a greater ability to precipitate and regulate the rate and consistency of crystal growth [14]. To study the sintering effect on the electrical properties, ferroelectric materials are often represented in terms of some complex parameters like complex impedance (Z^*), complex dielectric modulus (M^*), and loss tangent ($\tan\delta$) [15]. The real and imaginary parts of the impedance of the sample were measured simultaneously as a function of frequency. The main objective of this study is to take the measurements and analysis of materials in which ionic conduction with dipolar rotation is involved.

2. Experimental

2.1 Materials

Barium Calcium Zirconium Titanate, $x(\mathrm{Ba}_{0.85}\mathrm{Ca}_{0.15})\mathrm{TiO}_3$-$(1-x)\mathrm{Ba}(\mathrm{Zr}_{0.15}\mathrm{Ti}_{0.85})\mathrm{O}_3$ ($x = 0.4$, 0.5, 0.6) was prepared from Barium Acetate, $\mathrm{Ba(OH)_2{*}8H_2O}$ (Sigma Aldrich, 99% purity), Calcium Acetate, $(\mathrm{CH_3COO})_2\mathrm{Ca{*}}_X\mathrm{H_2O}$ (Sigma Aldrich, 99% purity) and Zirconyl Oxychloride ($\mathrm{ZrOCl_2{*}8H_2O}$) as starting materials. The sol was prepared by dissolving chemicals into 20 ml of de-ionized water with constant stirring. After stirring for 10 min at room temperature, Potassium Hydroxide (KOH), which acts as a mineralization agent, was added to the sol for maintaining pH. The solution was continuously stirred for 2 hours at room temperature, then transferred into the Teflon cup and the cup was placed within the reaction chamber, which was sealed and installed inside the furnace. The synthesis was carried out at 150 °C for 48 h (heating rate of 10 °C/min.). The crystalline powders were dried at 50 °C for 15 h.

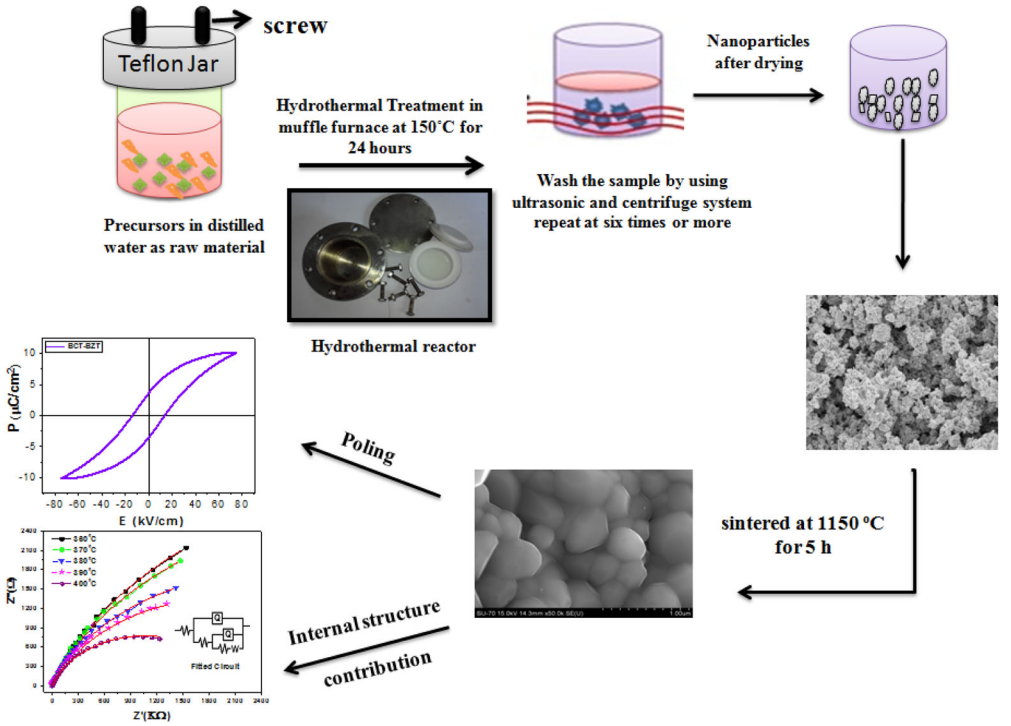

Figure 1. The comprehensive methodology of growth and various properties related to the material.

2.2 Characterization

The obtained powder samples were characterized by XRD using PW3040 Philips X-ray diffractometer with CuK_{α} radiation ($\lambda = 0.15406$ nm). The hydrothermally treated powders were milled and pressed into pellets by uniaxial pressing in a 10 mm die at 70 MPa. The pellets were sintered at 1150 °C for 5 h in a closed alumina crucible. The surface morphology and structure of these samples were characterized by using scanning electron microscopy SEM (JEO VP1450). For dielectric measurements, the sintered pellets were grounded and polished; silver paste was applied to opposite parallel faces, and coated pellets were fired in a furnace at 550 °C for 10 min for the formation of the electrode. The relative permittivity and loss tangent were recorded using an impedance analyzer (HP Agilent, 4192A Hewlett Packed) in the temperature range, 20 °C–400 °C.

3. Results and Discussion

3.1. Structural Study

Figure 2 shows the XRD pattern of $x(Ba_{0.85}Ca_{0.15})TiO_3$-$(1-x)Ba(Zr_{0.15}Ti_{0.85})O_3$. The pattern shows a polycrystalline perovskite nature; which is in good agreement with JCPDS#811289 data of $BaTiO_3$ ceramic material, and it shows that the samples have a tetragonal phase at room temperature. The main peak of the sample is located at approximately $2\theta = 31.480°$ having hkl value <110>.

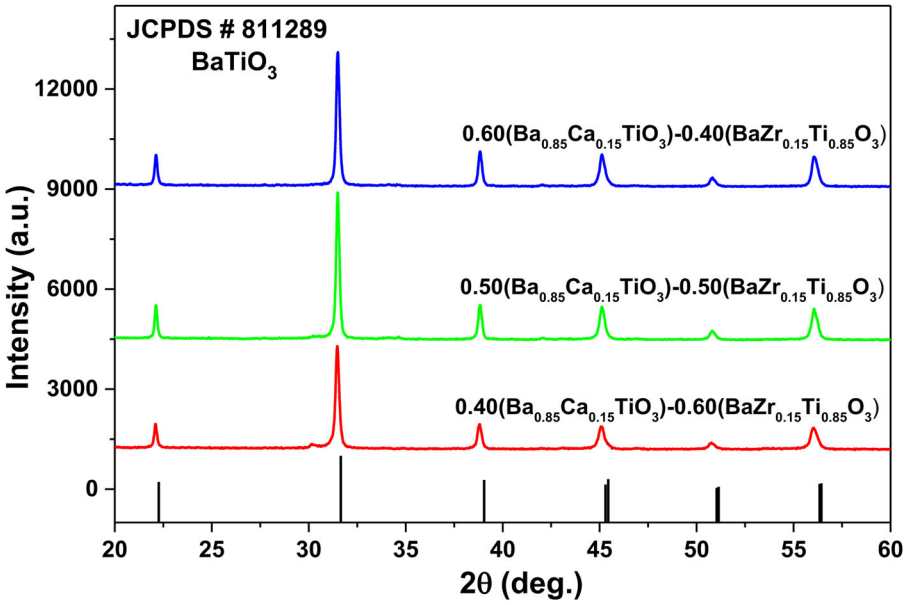

Figure 2. Room temperature XRD patterns of x(BCT)-(1–x)(BZT) (where $x = 0.4$, 0.5 and 0.6) ceramics.

The diffraction peaks of the compound were indexed in different crystal systems and unit cell configurations with the help of POWD [16]. The major reflection line in the XRD pattern is used for obtaining the average crystallite size by using the Debye–Scherrer equation [17] .

$$t = \frac{0.9\lambda}{\beta \cos\theta_B} \tag{1}$$

$$\beta = (\beta_M^2 - \beta_S^2)1/2 \tag{2}$$

where t is the crystallite size, λ is the X-ray wavelength (0.154 nm), β_M and β_S are the measured peak broadening and instrumental broadening in radian, respectively, and θ_B is the Bragg angle of the reflection. The calculated average crystallite size from Eq. (1) is 42.60 nm, 44.69 nm and 47.23 nm for the sample $x = 0.4$, $x = 0.5$ and $x = 0.6$, respectively. Comparison of different lattice parameter of x(BCT)-(1−x)(BZT) ceramics for $x = 0.4$, 0.5 and 0.6 has done at room temperature and mentioned in Table 1.

Figure 3 shows the SEM micrographs for x(BCT)-(1−x)(BZT) with $x = 0.4$, 0.5, 0.6. At low temperature, crystal growth and doping percentage of Zirconium and Calcium were proficient in apparent crystal formation and conscientious for consistent grains under suitable thermodynamic conditions. Roll of additives from solvent media in hydrothermal method, act as a binder between the particles and ease the self-assembly process [18,19]. The average particle size of BCT-BZT after hydrothermal treatment was 150 ± 30 nm. The sintering process is compiling of large grains due to matter transport mechanism and increases the grain size to ∼500 ± 50 nm for $x = 0.4$, ∼600 ± 50 nm for $x = 0.5$, ∼700 ± 50 nm for $x = 0.6$ (Fig. 2(d, f, e)).The density of the ceramics was found to be around 88% of the theoretical density.

Table 1. Comparison of lattice parameter of x(BCT)-(1−x)(BZT) ceramics for $x = 0.4$, 0.5 and 0.6 at room temperature.

	Lattice parameters					
Composition	a	b	c	c/a	V (Å^3)	esd
$BaTiO_3$(JCPDS#811289)	3.9842	3.9842	4.0256	1.0104	63.90	–
$0.4(Ba_{0.85}Ca_{0.15})TiO_3 - 0.6Ba(Zr_{0.15}Ti_{0.85})O_3$	3.6245	3.6245	4.5365	1.2516	56.44	0.006
$0.5(Ba_{0.85}Ca_{0.15})TiO_3 - 0.5Ba(Zr_{0.15}Ti_{0.85})O_3$	3.7235	3.7235	4.2960	1.1538	59.56	0.009
$0.6(Ba_{0.85}Ca_{0.15})TiO_3 - 0.4Ba(Zr_{0.15}Ti_{0.85})O_3$	3.9155	3.9155	4.1002	1.0472	62.82	0.003

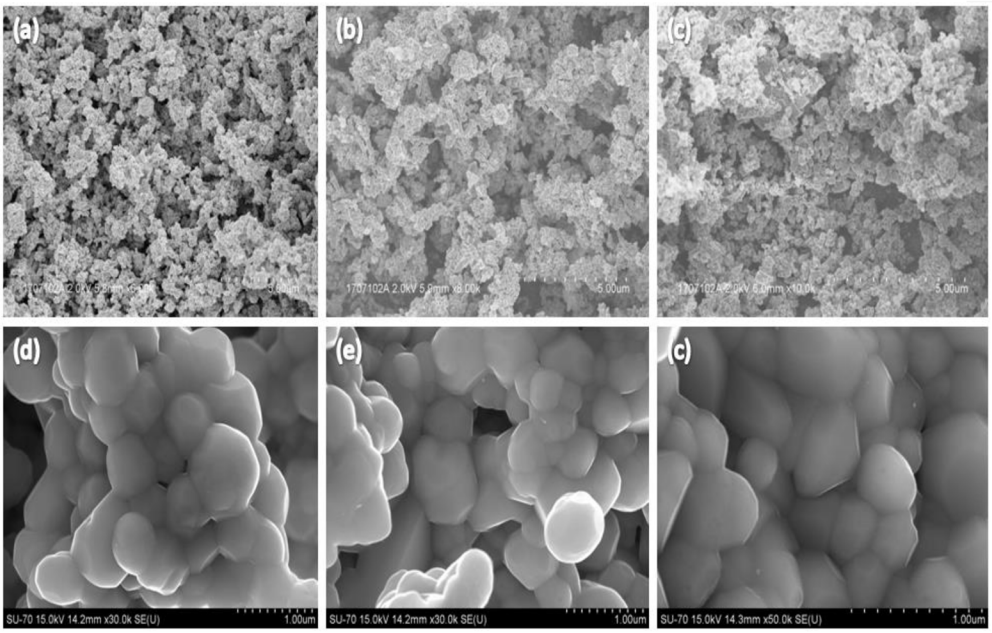

Figure 3. SEM images of x(BCT)-(1−x)(BZT) (where $x = 0.4$, 0.5 and 0.6) (a) powder produced by hydrothermal method at 150 °C (b) ceramics pellets sintered at 1150 °C.

3.2. Ferroelectric Study

Figure 4(a–c) shows the temperature dependence of dielectric constant (ε) of x(BCT)-(1−x) (BZT) (with $x = 0.4$, 0.5, 0.6) ceramics at different frequencies (1 kHz, 10 kHz and 100 kHz). Observed peaks show normal ferroelectric behavior explicitly and hence, the value of dielectric increases gradually with the increase in temperature up to the transition temperature and thereafter it decreases as the temperature was further increased. The transition was observed at following value of temperature ∼70 ± 10 °C for $x = 0.4$,∼100 ± 10 °C for $x = 0.5$, ∼100 ± 10 °C for $x = 0.6$. All the compositions demonstrated frequency-dependent dielectric response; as the peaks shifts with the increase in frequency. The peak values of dielectric constant (ε_r) at transition temperature are ∼2200 for the sample with $x = 0.4$, ∼1300 for the sample with $x = 0.5$, then relative permittivity increased up to ∼2600 for the sample with $x = 0.6$. At $x = 0.5$ BCT and BZT,

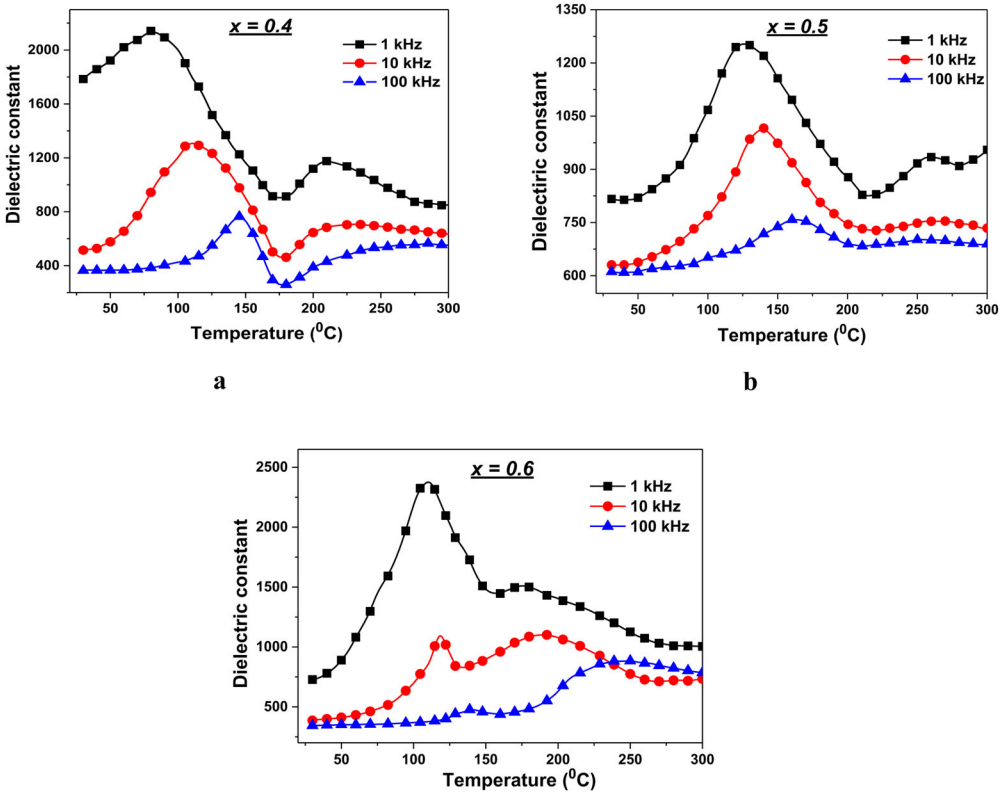

Figure 4. (a–c). Variation of dielectric constant of x(BCT)-(1 − x)(BZT) (where $x = 0.4$, 0.5 and 0.6) ceramics with temperature at frequency 1 kHz, 10 kHz and 100 kHz.

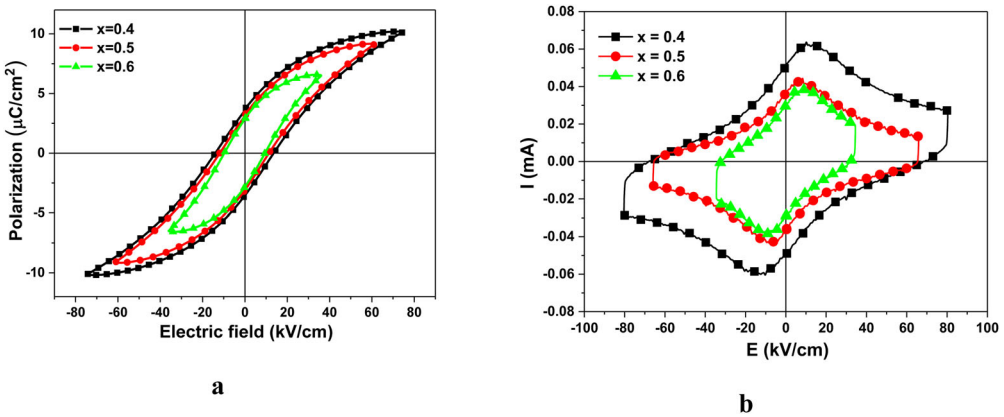

Figure 5. (a) Ferroelectric loop at different temperatures (b) Electric field dependence of polarization current of x(BCT)-(1−x)(BZT) (where $x = 0.4$, 0.5 and 0.6) ceramics at room temperature.

both were responsible for the phase transformation equally, which indicated that may be a percentage of tetragonality phase was decreasing in this sample.

Figure 5(a) shows the ferroelectric hysteresis loop of x(BCT)-(1−x) (BZT) (with $x = 0.4$, 0.5, 0.6) samples at 90 °C. All the samples exhibited saturated polarization with

Table 2. Comparison of ferroelectric hysteresis loop parameters of x(BCT)-(1−x)(BZT) ($x = 0.4$, 0.5 and 0.6)ceramics at room temperature.

Composition	P_S (Saturated Polarization) ($\mu C/cm^2$)	P_r (Remnant Polarization) ($\mu C/cm^2$)	E_C (Coercive Field) (kV/cm)
$0.4(Ba_{0.85}Ca_{0.15})TiO_3 - 0.6Ba(Zr_{0.15}Ti_{0.85})O_3$	11.65	5.49	19.58
$0.5(Ba_{0.85}Ca_{0.15})TiO_3 - 0.5Ba(Zr_{0.15}Ti_{0.85})O_3$	9.09	3.24	10.78
$0.6(Ba_{0.85}Ca_{0.15})TiO_3 - 0.4Ba(Zr_{0.15}Ti_{0.85})O_3$	6.50	2.99	9.57

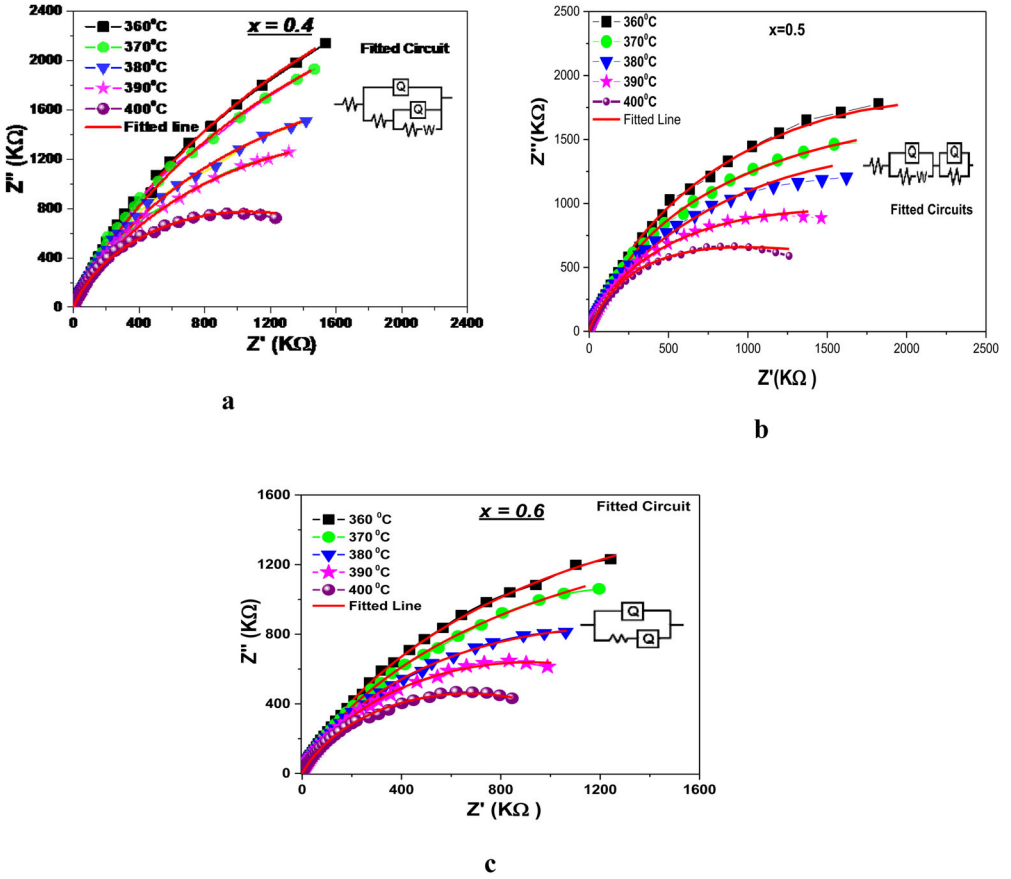

Figure 6. (a–c) Variation of real and imaginary part of impedance and Fitting of Cole-cole plot of x(BCT)-(1–x)(BZT) (where $x = 0.4$, 0.5 and 0.6) ceramics at different temperatures.

the applied field without any dielectric breakdown and show ferroelectric nature, which is the typical behavior of BCT-BZT ceramics [17]. The saturated polarization (P_s), remnant polarization (P_r) and the coercive field (E_c) confirmed the maximum polarization at above room temperature. For $x = 0.5$, there was a very small difference in between remnant polarization at room temperature and ferroelectric region, which evinced the thermal stability of the sample. The saturated and remnant polarization (P_S and P_r) at

Table 3. Parameters calculated from impedance fitted data $x(Ba_{0.85}Ca_{0.15})TiO_3$ - (1-x) $Ba(Zr_{0.15}Ti_{0.85})O_3$ (where x = 0.4, 0.5 and 0.6).

Sample	T (°C)	Resistance		Capacitance	N	Q
		R_g (Ω cm^2)	R_{gb} (Ω cm^2)	C_g (Fcm^2)		
$0.4(Ba_{0.85}Ca_{0.15})TiO_3$	360 °C	1.0×10^{-7}	8.732×10^{6}	–	7.88×10^{-1}	2.09×10^{-9}
$-0.6\ Ba(Zr_{0.15}Ti_{0.85})O_3$	370 °C	1.0×10^{-7}	7.536×10^{6}	–	7.834×10^{-1}	2.269×10^{-9}
	380 °C	1.0×10^{-7}	5.05×10^{6}	–	7.734×10^{-1}	2.628×10^{-9}
	390 °C	1.0×10^{-7}	3.97×10^{6}	–	7.93×10^{-1}	2.938×10^{-9}
	400 °C	1.0×10^{-7}	2.142×10^{6}	–	7.76×10^{-1}	2.375×10^{-9}
$0.5(Ba_{0.85}Ca_{0.15})TiO_3$	360 °C	1.0×10^{-7}	1.64×10^{6}	5.072×10^{-11}	6×10^{-1}	5.420×10^{-9}
$-0.5\ Ba(Zr_{0.15}Ti_{0.85})O_3$	370 °C	1.0×10^{-2}	2.52×10^{6}	5.113×10^{-11}	6.662×10^{-1}	5.101×10^{-9}
	380 °C	1.0×10^{-7}	2.05×10^{5}	5.146×10^{-11}	8.814×10^{-1}	5.275×10^{-9}
	390 °C	1.0×10^{-7}	1.887×10^{5}	5.157×10^{-11}	8×10^{-1}	1.232×10^{-9}
	400 °C	1.0×10^{-2}	1.749×10^{5}	5.207×10^{-11}	8.206×10^{-1}	1.056×10^{-9}
$0.6(Ba_{0.85}Ca_{0.15})TiO_3$	360 °C	1.0×10^{-2}	–	–	9.787×10^{-2}	1.56×10^{-7}
$-0.4\ Ba(Zr_{0.15}Ti_{0.85})O_3$	370 °C	1.0×10^{-7}	–	–	8.02×10^{-1}	1.365×10^{-10}
	380 °C	1.0×10^{-7}	–	–	7.83×10^{-1}	1.683×10^{-10}
	390 °C	1.0×10^{-7}	–	–	8×10^{-1}	3.284×10^{-9}
	400 °C	1.0×10^{-7}	–	–	8×10^{-1}	3.72×10^{-9}

room temperature of x(BCT)-(1−x) (BZT) ($x = 0.4$) sample were found to be 11.65 μC/cm^2 and 5.49 μC/cm^2 and coercive field (E_C) ~19.58 KV/cm. The high value of remnant polarization was attributed to any of the following: grain size, low defect density, compositional homogeneity and absence of domain-wall pinning centers, etc. [20,21]. With the increase in the content of Ca in x(BCT)-(1−x)(BZT), the ferroelectric loop exhibited a decrease in saturated polarization, remnant polarization and coercive field of x(BCT)-(1−x)(BZT) ($x = 0.5$) and x(BCT)-(1−x)(BZT) ($x = 0.6$), respectively [22]. Values of all the samples of saturated polarization (P_S), remnant polarization (P_r) and coercive field (E_C) are mentioned in Table 2.

Figure 5(b) shows electric field response of polarization current for x(BCT)-(1−x) (BZT) (where $x = 0.4$, 0.5, 0.6) samples. Polarized current shows a maximum of 0.065 mA for x(BCT)-(1−x) (BZT) ($x = 0.4$) sample. The curve decreases with the increase in electric field and reduces to zero for all the samples. x(BCT)-(1−x) (BZT) ($x = 0.4$) has a maximum value of current (I_P). However, the maximum value of polarized current is decreased with the increase in the content of Ca.

3.3. Impedance Study

The complex impedance spectroscopy technique was used to the role and the effects of different microstructural arrangement on the overall electrical proprieties of dielectric material [23]. Fig. 6(a–c) represents the temperature dependence of complex impedance spectrum Z′ versus Z″ of x(BCT)-(1−x) (BZT) (where $x = 0.4$, 0.5, 0.6) ceramics, which exhibits semicircular arc at high temperatures (360 °C–400 °C). The formation of single semicircle classifies the intrinsic grain contribution and intercept on the real axis (Z′) gives the value of bulk resistance (R_b) of the samples and retort in decrease with the rise in temperature. Bulk resistance (R_b) and bulk capacitance (C_b) offer the electrical behavior, which can be represented in terms of an equivalent circuit consisting of a series combination of parallel RC circuits [24]. The composition x(BCT)-(1−x) (BZT),

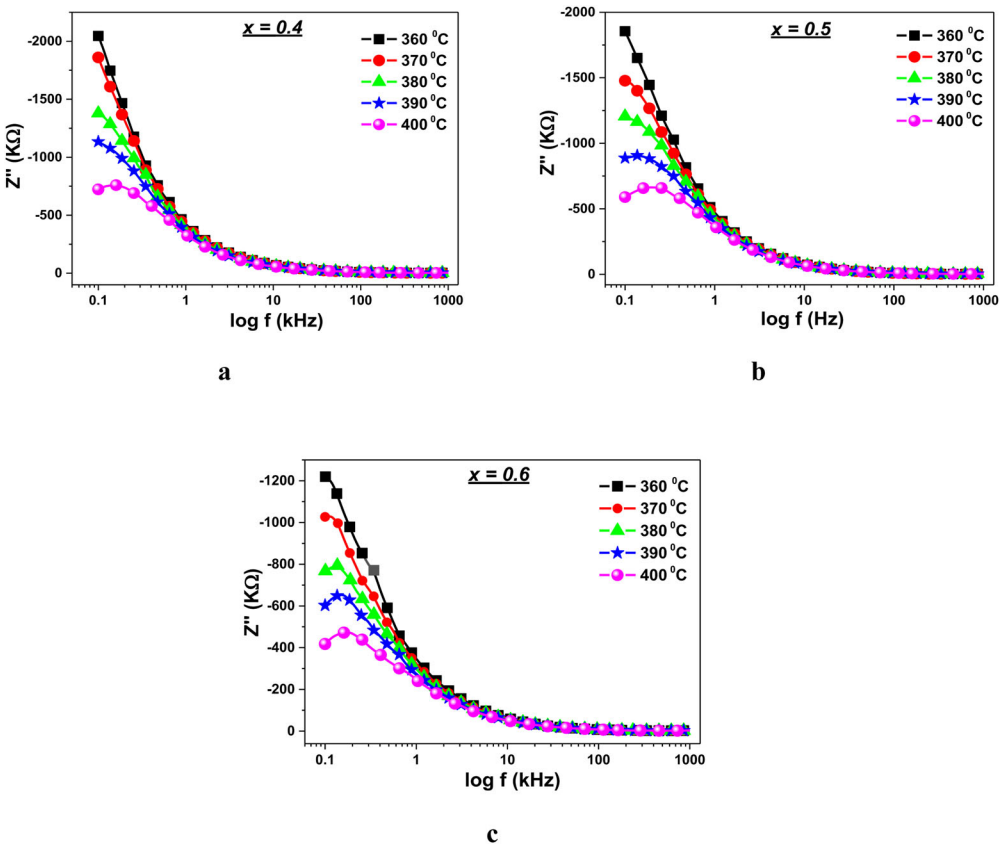

Figure 7. (a–c) Variation of imaginary part (Z″) of impedance with frequency at different temperatures of x(BCT)-(1−x)(BZT) (where $x = 0.4$, 0.5 and 0.6) ceramics.

$x = 0.5$ show some different characteristic, i.e. the variation in the equivalent circuit as a move toward higher temperature and show bulk capacitance (C_b) due to frequency corresponding peak of these semicircles. The depressed semicircles whose centers lie below the real axis indicated the departure from the ideal Debye behavior and exhibits the non-Debye type of relaxation phenomenon in the material [25]. The decrease in resistance with an increase in temperature revealed the reduction in charge barriers from the grains and grain boundaries so that with the increase in temperature, the conduction was enhanced [26]. Different parameters calculated from impedance fitted data for all samples are mentioned in Table 3.

Figure 7(a–c) shows the variation of the imaginary part of the impedance (Z″) as a function of frequency. The curves exhibited broad and low-intensity peaks with an insignificant shift toward the high-frequency region. It was given that bulk resistance decreases with the increase in frequency and gain relaxation at high temperatures (360 °C–400 °C). This reduction in bulk resistance with a rise in temperature exhibited the presence of relaxation process in the materials. At high frequencies, the perimeter of the grain boundary is affected due to low relaxation time [27,28]. Amalgamation of all peaks at high frequency indicated the presence of space charge polarization at lower frequency, whereas it disappears at higher frequency [29,30].

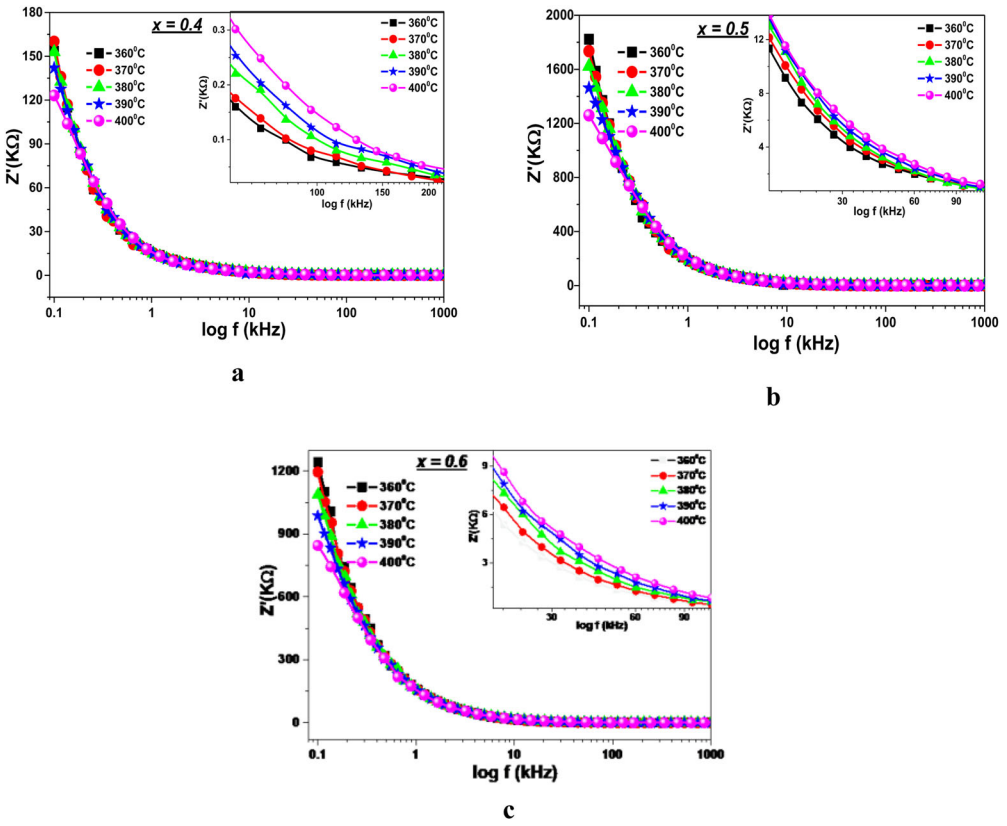

Figure 8. (a–c) Variation of imaginary part (Z′) of impedance with frequency at different temperatures of *x*(BCT)-(1−*x*)(BZT) (where $x = 0.4$, 0.5 and 0.6) ceramics.

Figure 8(a–c) shows the variation of the real part of impedance (Z′) as a function of frequency at different temperatures and compositions. The variation as a function of frequency in the low-frequency region followed by a saturation region in the high-frequency region. This suggests the continuation of dipolar polarization was not dominating and electronic as well as orientation polarization were activated in the mid-range of frequency to higher frequency [31]. In contrast, the decreasing trend of Z′ with the rise in temperature implied the presence of negative temperature coefficient of resistance (NTCR) in the material, which also indicated a possibility of an increase in ac-conductivity with the rise in temperature in the high-frequency region caused by the free space charge and inferior barrier properties of the material. In our studies, it was noted that ac conductivity is not increased so sharply because of the low concentration of oxygen vacancies during sintering that results in the charge reparation.

Figure 9(a–c) shows the normalized plot of Z''/Z''_{max} overlaps on a single master curve at a different temperature. It was clearly observed that the frequencies of *Z″ peaks* were coinciding having a similar shape as well as pattern in the peak position with slight variation in full width at half maximum (FWHM) with the rise in temperature. The dielectric processes occurring in the material were investigated via master Impedance plot, which concluded that for lower temperatures, the dynamical

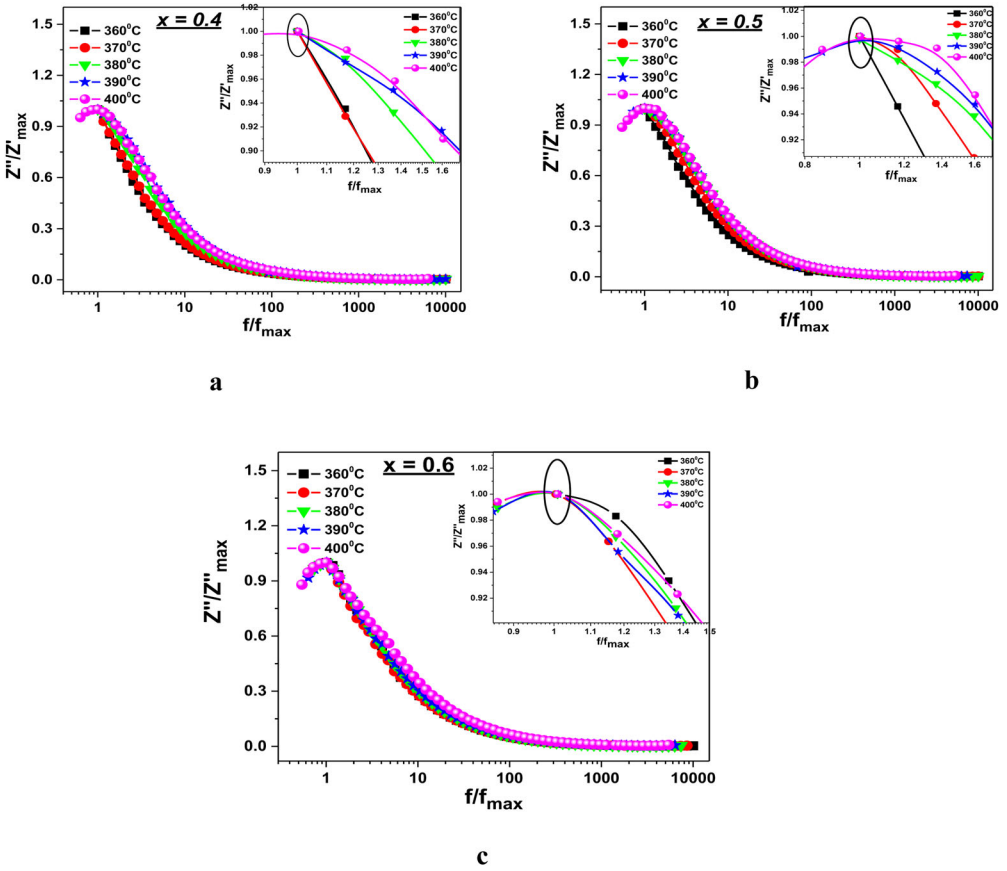

Figure 9. (a – c) Impedance scaling behavior of compounds in the master curves of *x*(BCT)-(1−*x*)(BZT) (where $x = 0.4$, 0.5 and 0.6) ceramics.

processes were nearly temperature independent [25,32]. It was also observed that the Z''/Z''_{max} curves were non-symmetric, which further implied a non-exponential behavior of the conductivity relaxation. The FWHM of the spectra is wider than the breadth of a Debye peak, which suggested the presence of a non-Debye type of relaxation phenomenon.

Figure 10(a–c) shows two semicircular arcs at each of the high temperatures (above 360 °C–400 °C) were observed, which suggested the presence of bulk and grain boundary within the synthesized materials. It also observed that the semicircle arc was almost the same at high frequency and low-frequency region at all the temperatures. The modulus spectrum shows stability in the shape with the rise in temperature, which clearly indicated no apparent change in the capacitance value as a function of temperature. The observed pattern of modulus graph confirmed the subsistence of the hopping mechanism in the electrical conduction of the synthesized materials. On the increasing temperature, the intercept on M′ axis shifts toward the higher value of M″ and thus indicated the increase in capacitance, which supported the negative temperature coefficient of resistance type behavior of the materials since bulk capacitance (C_b) is inversely proportional to the bulk resistance (R_b).

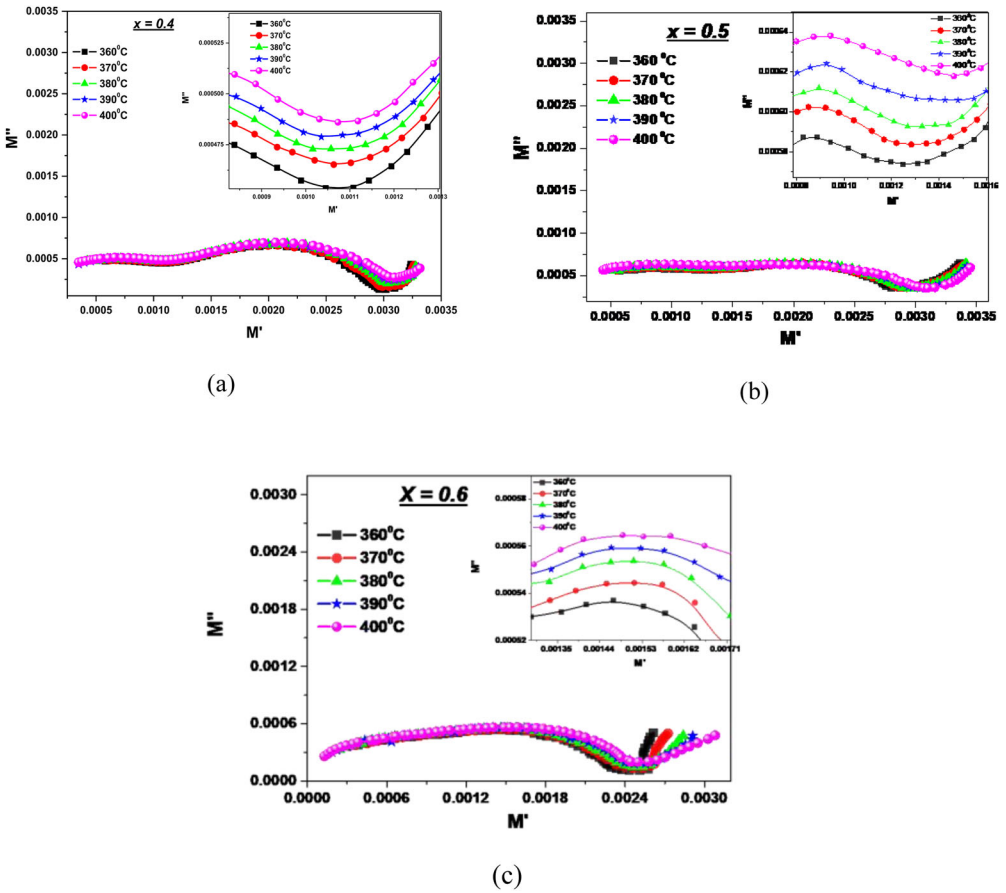

Figure 10. (a–c) Variation of real and imaginary part of modulus at different temperatures of x(BCT)-(1−x)(BZT) (where $x = 0.4$, 0.5 and 0.6) ceramics.

4. Conclusions

(BCT)-(1−x) (BZT) (where $x = 0.4$, 0.5 and 0.6) ceramics were prepared via hydrothermal reaction method. XRD patterns of the pure perovskite phase suggested tetragonal structure at room temperature. All the aforementioned compositions exhibited saturated polarization with an applied electric field and show soft ferroelectric nature. Real and imaginary parts of complex impedance and modulus properties substantiate the relaxation process at high frequency. Impedance analysis indicated the presence of mostly bulk (grain) resistive contributions in the synthesized materials at higher temperatures, whereas complex modulus plots show the presence of grains as well as grain boundary contributions in the materials. Both impedance and modulus analysis prop up the typical NTCR behavior. Effect of temperature on bulk resistance also confirmed the presence of a non-Debye type of relaxation phenomenon in the materials.

Acknowledgments

S. Thakur also acknowledges I3N and FCT for the post-doc grant with reference BPD-14/I3N (7908/2017).

Funding

The authors are grateful by the FEDER funds through the COMPETE 2020 Program and National Funds through FCT - Portuguese Foundation for Science and Technology under the project UID/CTM/50025/2013.

References

1. X. Cheng *et al.*, Hydrothermal solvothermal synthesis and microwave absorbing study of MCo_2O_4 (M = Mn, Ni) microparticles, *Adv. Appl. Ceram.* **118** (8), 466 (2019). DOI: 10.1080/17436753.2019.1667174.
2. F. Kröger and H. Vink, Relations between the concentrations of imperfections in crystalline solids, in *Solid State Physics* (Elsevier, 1956), pp. 307–435.
3. Z-h Chen *et al.*, Piezoelectric and ferroelectric properties of $Ba_{0.9}Ca_{0.1}Ti_{0.9}Sn_{0.1}O_3$ lead-free ceramics with La_2O_3 addition, *J. Alloys Compd.* **704**, 193 (2017). DOI: 10.1016/j.jallcom.2017.01.237.
4. D. Damjanovic *et al.*, What can be expected from lead-free piezoelectric materials? *Funct. Mater. Lett.* **3** (1), 5 (2010). DOI: 10.1142/S1793604710000919.
5. P. Kantha *et al.*, Phase formation and electrical properties of BNLT–BZT lead-free piezoelectric ceramic system, *Curr. Appl. Phys.* **9** (2), 460 (2009). DOI: 10.1016/j.cap.2008.04.004.
6. W. Liu and X. Ren, Large piezoelectric effect in Pb-free ceramics, *Phys. Rev. Lett.* **103** (25), 257602 (2009). DOI: 10.1103/PhysRevLett.103.257602.
7. S. Q. Jan *et al.*, A study of relaxation effects in (1-x)$BaZr_{0.2}Ti_{0.8}O_{3-x}Ba_{0.7}Ca_{0.3}$, TiO_3 (x = 0.3, 0.35, 0.4) ferroelectric ceramics, *J. Alloys Compd.* **735**, 1893 (2018). DOI: 10.1016/j.jallcom.2017.11.275.
8. M. Shandilya *et al.*, Modification of structural and electrical properties of Ca element on barium titanate nano-material synthesized by hydrothermal method, *Ferroelectrics* **520** (1), 93 (2017). DOI: 10.1080/00150193.2017.1375323.
9. S. Shalu and B. D. Ghosh, Synthesis, characterization and dielectric properties of low-loss Zr-doped barium strontium titanate materials, *Adv. Appl. Ceram.* **118** (8), 451 (2019). DOI: 10.1080/17436753.2019.1664793.
10. S. Vasawade *et al.*, Structural and dielectric properties of lead-free Zr-doped barium titanates, *Int. J. Self-Propag. High-Temp. Synth.* **27** (1), 26 (2018). DOI: 10.3103/S1061386218010119.
11. H. Bao *et al.*, A modified lead-free piezoelectric BZT–xBCT system with higher TC, *J. Phys. D: Appl. Phys.* **43** (46), 465401 (2010). DOI: 10.1088/0022-3727/43/46/465401.
12. S. Su *et al.*, Poling dependence and stability of piezoelectric properties of Ba $(Zr_{0.2}Ti_{0.8})$ O_3-$(Ba_{0.7}Ca_{0.3})$ TiO_3 ceramics with huge piezoelectric coefficients, *Curr. Appl. Phys.* **11** (3), S120 (2011). DOI: 10.1016/j.cap.2011.01.034.
13. M. Shandilya, R. Rai, and J. Singh, Review: hydrothermal technology for smart materials, *Adv. Appl. Ceram.* **115** (6), 354 (2016). DOI: 10.1080/17436753.2016.1157131.
14. M. Shandilya, R. Rai, and A. Zeb, Structural and dielectric relaxor properties of $Ba_{1-x}Mg_xTiO_3$ ceramics prepared through a hydrothermal route, *Adv. Appl. Ceram.* **117** (5), 255 (2018). DOI: 10.1080/17436753.2017.1405557.
15. N. Singh *et al.*, Dielectric relaxation, electrical conductivity and impedance response of barium titanate (BT) and strontium titanate (ST) doped Ba $(Fe_{0.5}Nb_{0.5})O_3$ ceramics, *J Eng. Technol. Res.* **4**, 104 (2012).
16. E. Wu, POWD, an interactive program for powder diffraction data interpretation and indexing, *J. Appl. Crystallogr.* **22** (5), 506 (1989). DOI: 10.1107/S0021889889005066.
17. J. P. Praveen *et al.*, Effect of poling process on piezoelectric properties of sol–gel derived BZT–BCT ceramics, *J. Eur. Ceram. Soc.* **35** (6), 1785 (2015)., DOI: 10.1016/j.jeurceramsoc.2014.12.010.

18. M. Shandilya and G. A. Kaur, Low temperature crystal growth of lead-free complex perovskite nano-structure by using sol-gel hydrothermal process, *J. Solid State Chem.* **280**, 120988 (2019). DOI: 10.1016/j.jssc.2019.120988.
19. M. Shandilya, S. Thakur, and R. Rai, Study of phase transitional behavior and electrical properties of relaxor $Ba_{0.85}Ca_{0.15}Zr_{0.05}Ti_{0.95}O_3$ lead free ceramic, *Ferroelectr. Lett. Sect.* **46** (1-3), 8 (2019). DOI: 10.1080/07315171.2019.1647705.
20. A. Manjón-Sanz *et al.*, Total scattering and diffraction studies of lead-free piezoelectric (1-x)$Ba(Zr_{0.2}Ti_{0.8})O_{3-x}$ ($Ba_{0.7}Ca_{0.3}$) TiO_3 deconvolute intrinsic and extrinsic contributions to electromechanical strain, *Acta Mater.* **171**, 79 (2019). DOI: 10.1016/j.actamat.2019.04.005.
21. A. Patra *et al.*, Enhanced dielectric, ferroelectrics and piezoelectric behavior of tape casted BCT–BZT piezoelectric wafer, *J. Mater. Sci: Mater. Electron.* **29** (16), 14046 (2018)., DOI: 10.1007/s10854-018-9536-8.
22. V. S. Puli *et al.*, Barium zirconate-titanate/barium calcium-titanate ceramics via sol–gel process: novel high-energy-density capacitors, *J. Phys. D: Appl. Phys.* **44** (39), 395403 (2011)., DOI: 10.1088/0022-3727/44/39/395403.
23. S. Belkhadir *et al.*, Impedance spectroscopy analysis of the diffuse phase transition in lead-free $(Ba_{0.85}Ca_{0.15})(Zr_{0.1}Ti_{0.9})O_3$ ceramic elaborated by sol-gel method, *Superlattices Microstruct.* **127**, 71 (2019). DOI: 10.1016/j.spmi.2018.03.009.
24. S. K. Patri *et al.*, Dielectric, impedance and modulus spectroscopy of $BaBi_2Nb_2O_9$, *J. Electroceram.* **40** (4), 338 (2018). DOI: 10.1007/s10832-018-0135-0.
25. A. Shukla, R. Choudhary, and A. Thakur, Effect of Mn^{4+} substitution on thermal, structural, dielectric and impedance properties of lead titanate, *J. Mater. Sci: Mater. Electron.* **20** (8), 745 (2009). DOI: 10.1007/s10854-008-9797-8.
26. S. Li *et al.*, Effect of composition fluctuation on structural and electrical properties of BZT-xBCT ceramics prepared by plasma activated sintering, *J. Eur. Ceram. Soc.* **37** (5), 2067 (2017). DOI: 10.1016/j.jeurceramsoc.2016.12.043.
27. M. R. Raju and R. Choudhary, Effect of Zr+ 4 ion substitution on the structural, dielectric and electrical properties of $Sr_5LaTi_3Nb_7O_{30}$ ceramics, *J. Mater. Sci.* **39** (5), 1765 (2004). DOI: 10.1023/B:JMSC.0000016182.42768.cf.
28. R. Ranjan *et al.*, Structural and impedance spectroscopic studies of samarium modified lead zirconate titanate ceramics, *Phys B Condens Matter* **404** (20), 3709 (2009). DOI: 10.1016/j.physb.2009.06.113.
29. T. Badapanda *et al.*, Structural and impedance spectroscopy study of Samarium modified Barium Zirconium Titanate ceramic prepared by mechanochemical route, *Curr. Appl. Phys.* **14** (9), 1192 (2014). DOI: 10.1016/j.cap.2014.06.007.
30. A. Mahmood, Y. Iqbal, and A. Ullah, Phase, microstructure and electrical characterization of $Ba_{1-x}La_x$ $(Zr_{0.6}Ti_{0.4})_{1-x/4}O_3$ ceramics, *J. Mater. Sci: Mater. Electron.* **26** (1), 113 (2015). DOI: 10.1007/s10854-014-2371-7.
31. Y. Huang *et al.*, Understanding the validity of impedance and modulus spectroscopy on exploring electrical heterogeneity in dielectric ceramics, *J. Appl. Phys.* **125** (8), 084103 (2019)., DOI: 10.1063/1.5081842.
32. R. Ranjan *et al.*, Structural, dielectric and transport properties of $(PbSm)(ZrTi)O_3$ ceramics, *Mod. Phys. Lett. B* **23** (15), 1947 (2009). DOI: 10.1142/S0217984909019983.